

Dynamic Photocontrol of the Coffee-Ring Effect with Optically Tunable Particle Stickiness**

Manos Anyfantakis and Damien Baigl*

Abstract: When a colloidal drop dries on a surface, most of the particles accumulate at the drop periphery, yielding a characteristic ring-shaped pattern. This so-called coffee-ring effect (CRE) is observed in any pinned evaporating drop containing non-volatile solutes. Here, the CRE is dynamically controlled for the first time by using light, and an unprecedented reconfigurability of the deposit profile is demonstrated. This is achieved through a new mechanism where particle stickiness is optically tuned on demand, thus offering reliable modulation of the deposition pattern. The system consists of anionic nanoparticles and photosensitive cationic surfactants dispersed in water. It is shown that light-dependent modulation of surfactant–particle interactions dictates particle attraction and trapping at the liquid–gas interface, which allows us to direct particle deposition into a wide range of patterns from rings to homogeneous disks. Patterning from single drops is photo-reversible upon changing the wavelength whereas spatial control in multiple drop arrays is achieved using a photomask.

The coffee-ring effect (CRE) is a ubiquitous phenomenon observed for pinned drying drops containing virtually any kind of non-volatile solutes, including a broad range of synthetic and biological materials.^[1] Owing to its robustness, the CRE has been frequently harnessed for patterning solutes on surfaces.^[2] On the contrary, it can be an obstacle in numerous applications that require homogenous solute deposition,^[1c,3] leading researchers to intensively seek ways to control the CRE.^[4] However, despite its phenomenologically simple nature, the CRE is a complex process involving

phenomena at different length scales, such as bulk and surface flows, particle–particle and substrate–particle interactions, as well as contact line dynamics.^[1a,5] Most of the methods reported thus far for controlling the CRE have relied on adapting drop composition^[6] and solute characteristics,^[7] hindering any reconfigurability for a given system.

Addressing this challenge, we designed a system exhibiting photodependent particle stickiness by adding a photosensitive surfactant (AzoTAB) to aqueous suspensions with a fixed concentration (2 mg mL⁻¹) of negatively charged polystyrene nanoparticles (NPs; Figure 1 a). AzoTAB is an amphiphilic molecule composed of a cationic head and a hydrophobic tail containing an azobenzene moiety, which photoisomerizes between its *trans* (less polar) and *cis* (more polar) states upon blue and UV irradiation, respectively^[8] (Supporting Information, Figure S1). Drops of these suspensions (μ L amounts) were deposited on glass coverslips and illuminated with UV ($\lambda = 365$ nm) or blue ($\lambda = 440$ nm) LED light for a specific amount of time; then, the drops were left to evaporate in the dark. In a first experiment, three arrays of a total number of 65 identical drops ($[AzoTAB] = 1$ mM) were irradiated simultaneously with UV light for five minutes through a photomask forming the three letters E, N, and S (Figure 1 b). A typical coffee ring was observed for all droplets protected from UV irradiation (Figure 1 c, Figure 1 d, right, and Movie S1); this implies that the NPs were mainly concentrated in the drop periphery after the evaporation was completed. In contrast, all droplets exposed to UV light resulted in a markedly different deposition pattern: After drop drying, a homogeneous disk was reproducibly observed (Figure 1 d, left). These results show that in the presence of a photosensitive cationic surfactant, short-time UV illumination of a colloidal suspension dramatically affects the evaporation-driven deposition of anionic particles. This effect can be exploited for organizing particles on a solid substrate along predefined patterns.

To emphasize the role of AzoTAB and to get further insight into the mechanism at the origin of particle distribution, we varied the AzoTAB concentration, keeping the NP concentration fixed at 2 mg mL⁻¹. We measured the effective surface potential (ζ) of the particles for suspensions being exposed to ambient ($-UV$ conditions) or 365 nm ($+UV$ conditions) light (Figure 2 a). For the surfactant-free dispersions ($[AzoTAB] = 0$ mM), ζ assumed a value of approximately -50 mV, regardless of the illumination conditions, showing a high density of negative charges on the NP surface as well as the absence of intrinsic light sensitivity. In the presence of AzoTAB and without UV irradiation, the ζ value increased with an increase in AzoTAB concentration, became 0 mV at approximately $[AzoTAB] = 0.1$ mM, and reached

[*] Dr. M. Anyfantakis, Prof. D. Baigl
Department of Chemistry
Ecole Normale Supérieure, PSL Research University
24 rue Lhomond, F-75005, Paris (France)
and
Sorbonne Universités, UPMC Univ Paris 06, PASTEUR
F-75005, Paris (France)
and
CNRS, UMR 8640 PASTEUR
F-75005, Paris (France)
E-mail: damien.baigl@ens.fr
Homepage: <http://www.baigllab.com/>

[**] We thank H. El-Deen Sharaf and U. Jonas for providing the anionic polystyrene nanoparticles, J. Fattaccioli, K. Jaskiewicz, and A. Bourgeault for experimental support, O. Gang and S. Granick for comments on the manuscript, and S. Rudiuk for discussion. This work was supported by the European Research Council (ERC) [European Community's Seventh Framework Programme (FP7/2007–2013), ERC Grant agreement 258782], the Mairie de Paris (Emergence(s) 2012), and the Institut Universitaire de France (IUF).



Supporting information for this article is available on the WWW under <http://dx.doi.org/10.1002/anie.201406903>.

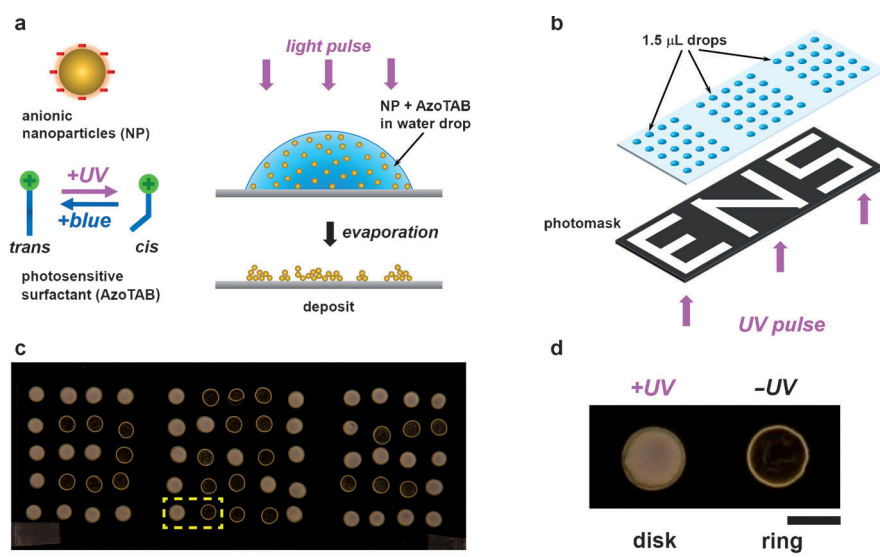


Figure 1. Light controls the formation of either a ring- or a disk-shaped deposit from individual evaporating drops, thus allowing spatial patterning in a drop array. a) The main experiment consists of 1) illuminating a sessile water drop containing negatively charged nanoparticles (NPs, 500 nm diameter, 2 mg mL^{-1}) and a photosensitive azobenzene trimethylammonium bromide (AzoTAB) cationic surfactant and 2) letting it evaporate until a solid deposit is formed. b) Illumination at 365 nm for 5 minutes of an array of 65 identical drops ($1.5 \mu\text{L}$, $[\text{AzoTAB}] = 1 \text{ mM}$) through a photomask. c) Photograph of the resulting pattern after complete evaporation of all of the drops. d) Magnified image of the area indicated by dashed lines in (c), showing a disk- and a ring-shaped pattern for drops initially exposed to (+UV) and protected from (-UV) the light stimulus. Scale bars are 10 mm and 2 mm for (c) and (d), respectively.

values of about +20 mV for $[\text{AzoTAB}] = 5 \text{ mM}$. It is known that the adsorption of cationic surfactants to negatively charged particles can alter and even reverse the surface charge because of electrostatic and hydrophobic interactions.^[9] Interestingly, a similar charge increase was observed under UV irradiation, but the curve was significantly shifted to higher AzoTAB concentrations, resulting in smaller ζ values for $0.03 \leq [\text{AzoTAB}] \leq 5 \text{ mM}$, and a charge reversal occurring at an AzoTAB concentration of approximately 0.25 mM. It has already been shown that a surfactant with higher polarity leads to less cooperative adsorption and therefore a decrease in the ζ value of surfactant/NP mixtures.^[10] Here, UV irradiation induced an isomerization of AzoTAB to its more polar *cis* form, which decreased its binding ability to the particles. This result implies that for a given composition, UV irradiation led to a reduction in the surface charge of the particles, but for both illumination conditions, positive ζ values were measured at sufficiently high AzoTAB concentrations. Large absolute ζ values indicate well-stabilized particles (referred to as non-sticky), owing to the dominance of repulsive interactions, whereas values close to 0 mV correspond to particles with a tendency to aggregate and adsorb at the liquid–gas (LG) interface^[11] (referred to as sticky). NPs were thus successively non-sticky (highly negative), sticky (almost neutral), and non-sticky (highly positive) when the AzoTAB concentration increased for both the -UV and the +UV conditions, but the surfactant concentration range corresponding to sticky particles strongly depended on the illumination conditions (Figure 2b). As

a consequence, although stickiness was not affected by UV light for the lowest and highest AzoTAB concentrations, UV light induced a transition from sticky to non-sticky particles, and vice versa, at intermediate AzoTAB concentrations. Therefore, in this concentration range, NP/AzoTAB mixtures behave as suspensions with optically tunable particle stickiness.

By systematically analyzing the deposition patterns after evaporation was completed, we found that the deposit morphology was first a ring, then a disk, and finally a ring again, when the AzoTAB concentration was increased from 0 to 5 mM for both -UV and +UV conditions (Figure 2c). However, the concentration range to get a disk-like profile strongly depended on the illumination conditions, with values of 0.05–0.1 mM and 0.25–1 mM under -UV and +UV conditions, respectively. Strikingly, for both illumination conditions, the disk-like profile was obtained for ζ values close to 0 mV, which corresponds to sticky particles, whereas a ring-shaped profile was observed for highly negatively or highly positively charged surfaces, that is, non-sticky particles. These results show the direct correlation between particle stickiness and deposit morphology. As a consequence, UV light had no effect at very low and very high AzoTAB concentrations where particles were non-sticky and formed a ring-shaped pattern (Figure 2c, left and right panels). In contrast, UV irradiation induced a disk→ring transition for $[\text{AzoTAB}] = 0.05\text{--}0.1 \text{ mM}$ (Figure 2c, middle left panels) by switching the properties of the NPs from sticky to non-sticky, and a ring→disk transition for $[\text{AzoTAB}] = 0.25\text{--}1 \text{ mM}$ (Figure 2c, middle right panels) by switching the NPs from non-sticky to sticky. These results show that light controls the deposition of particles through its impact on their stickiness.

In all of our experiments, the drop contact line was either firmly pinned on the glass substrate directly after deposition, or, in some cases, receded for a few seconds after deposition (maximum displacement ca. $30 \mu\text{m}$) and then remained pinned during the evaporation process. The radially outward capillary flow was thus in all cases transporting NPs to the drop contact line, where the evaporation rate was the highest (Movie S2). This flow also accumulated surfactants at the drop periphery, inducing an inward Marangoni flow pointing from the contact line to the drop apex owing to the resulting surfactant gradient at the LG interface. Other groups have reported that Marangoni flows could be strong enough to compensate for the outward capillary flow and rehomogenize particles inside an evaporative drop, but this was typically achieved at surfactant concentrations close to or larger than the critical micellar concentration (CMC).^[6a] In our experi-

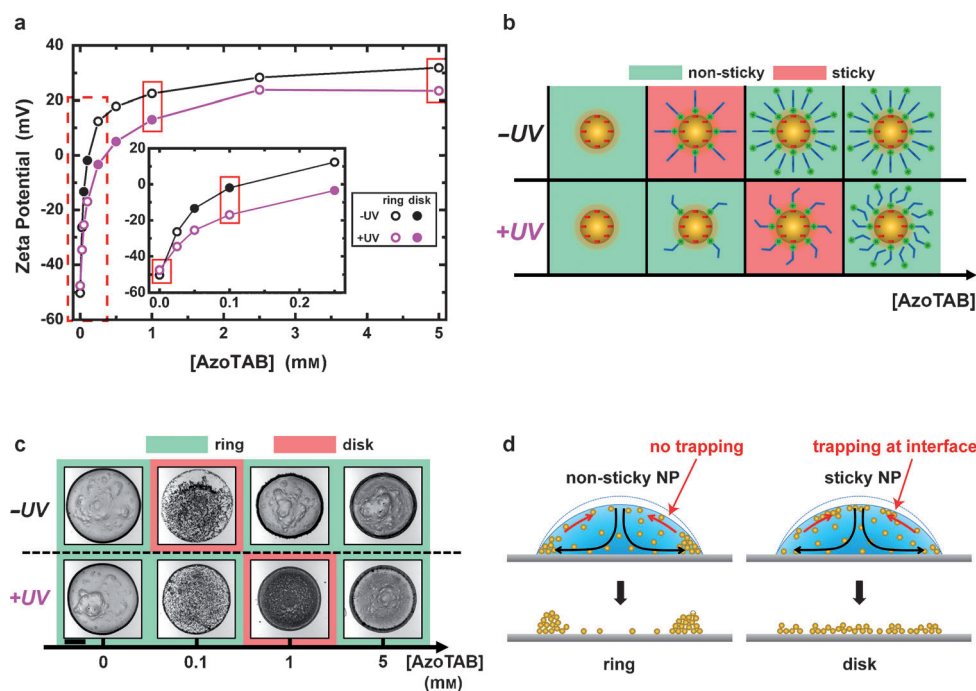


Figure 2. Photodependent particle stickiness allows for various light-induced transitions between ring- and disk-shaped deposits as a function of AzoTAB concentration. a) Zeta potentials (ζ) of the NPs for various AzoTAB concentrations, without (–UV, black) or with (+UV, violet) illumination at 365 nm prior to measurement in the dark. Symbols are mean values of three independent measurements with error bars (\pm sd) smaller than the symbol size. Open and filled symbols indicate deposits displaying ring- or disk-shaped morphologies, respectively. The inset shows a magnified image of the part indicated by the dashed box. b) ζ Measurements indicate that NPs are initially highly negative and non-sticky, become sticky upon charge neutralization by AzoTAB, and are non-sticky again once they are overcharged by AzoTAB. The AzoTAB concentration range to get sticky NPs depends on the AzoTAB isomerization state, with the *cis* isomer (+UV) being less efficient in neutralizing NPs than the *trans* isomer (–UV). c) Representative micrographs of the deposits obtained for the AzoTAB concentrations and illumination conditions indicated by the red boxes in (a). Scale bar: 500 μ m. d) We suggest that the Marangoni flow (red arrows) is not strong enough to compensate for the evaporation-driven capillary flow (black arrows), which transports particles towards the contact line. As a consequence, a ring-shaped pattern is obtained after evaporation in all cases that involve non-sticky particles (left). In contrast, sticky particles are trapped at the liquid–gas interface during their circulation, which results in a more homogeneous, disk-shaped deposit (right) after evaporation.

ments, the Marangoni flow was not strong enough to counteract the outward capillary flow, probably because the AzoTAB concentrations were always smaller than the CMC (12.6 and 14.6 mM for the *trans* and *cis* isomers, respectively^[12]). Therefore, regardless of the AzoTAB concentration, in the case of non-sticky particles, a ring was always obtained (Figure 2d, left). In the case of sticky particles, a similar circulation flow occurred but the LG interface could trap individual or clustered particles, which were distributed at the LG interface rather than accumulating at the drop periphery. Note that the formation of such arrested clusters at the LG interface was always observed for the sticky particles (Movie S3). As a result, a homogeneous distribution on the surface, that is, a disk-shaped pattern, was obtained after complete evaporation (Figure 2d, right). Our suggested mechanism is supported by a series of control experiments using cationic NPs of similar size (Figure S2), a non-photosensitive surfactant (Figure S3), and polystyrene substrates^[13] (Figure S4).

We then focused on the UV-induced ring→disk transition by keeping the AzoTAB concentration at 1 mM, and we studied its kinetic behavior by varying the UV irradiation time after drop deposition. Without UV irradiation, the usual ring-shaped pattern was observed (Figure 3a, left). Under our conditions, about 200 seconds of UV exposure were enough to get a rather homogenous deposition (Figure 3a, right), whereas shorter illumination times resulted in intermediate patterns (Figure 3a, middle panels). A systematic analysis of the average radial profile of the deposit (Figure S5) showed that the excess of particles at the droplet periphery, which is responsible for the ring formation, progressively decreased with UV exposure time while the droplet interior was covered with an increasing amount of particles (Figure 3b). From the deposit profile, we computed the ring factor (RF); a high value means that most particles are located at the drop periphery (ring pattern), whereas a value close to zero represents homogeneous deposition (disk pattern; see Figure S5). We found that the RF values continuously decreased from approximately

0.4 (ring) to nearly 0 (disk) with an increase in UV illumination time (Figure 3c), which emphasizes the ability to finely tune the deposit profile by simply adjusting the UV dose. Strikingly, by absorption measurements, we found that the UV-induced *trans*–*cis* isomerization of AzoTAB inside the drop had a kinetic evolution identical to that of the ring factor (Figure S6). This shows that light controls the *trans/cis* composition of AzoTAB in solution, which in turn modulates the particle stickiness, thus directing the deposition behavior.

Finally, as the AzoTAB *trans*–*cis* photoisomerization under UV light is reversible upon blue-light irradiation (Figure S1), we applied cycles of UV/blue light exposure on several identical drops ([AzoTAB] = 1 mM) immediately after drop deposition and analyzed the deposit profile after complete evaporation of each drop. Interestingly, we found that the final deposit was reversibly switched between a disk- and a ring-shaped pattern after successive applications of UV and blue light, respectively (Figure 4). Under our conditions,

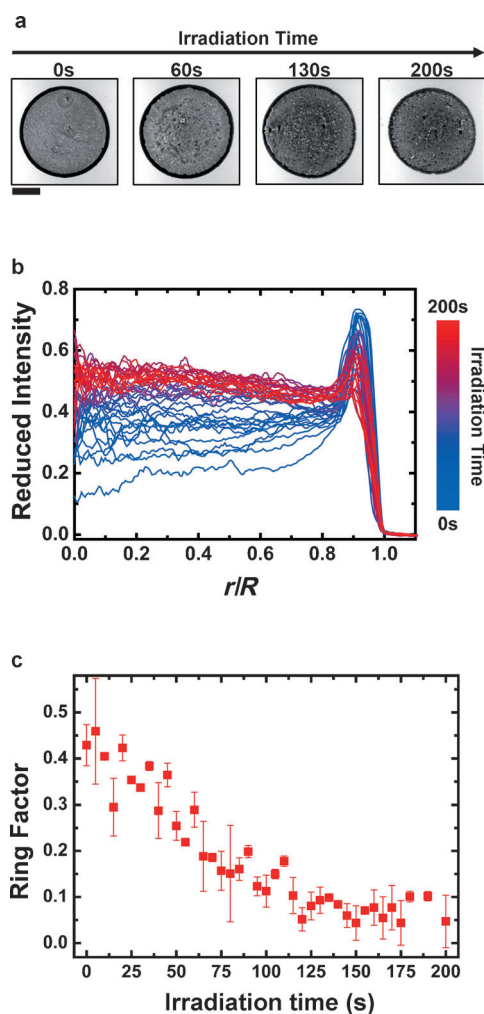


Figure 3. The UV irradiation time finely tunes the deposit into a variety of shapes ranging from a ring to a homogenous deposition pattern. a) Representative micrographs of the deposits obtained at [AzoTAB]=1 mM and various irradiation times at 365 nm on 0.8 μL drops. Scale bar: 500 μm . b) Average radial profile of the deposit, determined according to Figure S5, with r being the distance from the drop center (radial coordinate) and R the deposit radius, for different irradiation times as indicated by the color code. c) Ring factor (RF) computed by comparing the intensity at the ring position with that at the drop interior (see Figure S5) as a function of the irradiation time. Symbols and error bars show mean \pm SD values for three drops.

three full cycles could be carried out. These results demonstrate the dynamic control of the coffee-ring effect and confirm the role of the photoreversible AzoTAB isomerization in controlling the deposition process through photo-dependent surfactant binding to the particles.

In conclusion, we have designed a photoresponsive suspension composed of anionic colloids and a photosensitive surfactant, where the particle–surfactant interactions were reversibly and finely tuned by an LED light stimulus. As a result, particle stickiness was optically controlled, and we demonstrated how it in turn directed particle deposition upon evaporation. Looking forward, we anticipate stimuli-responsive stickiness to be a starting point for the development of general strategies to tailor particle organization at ultimately

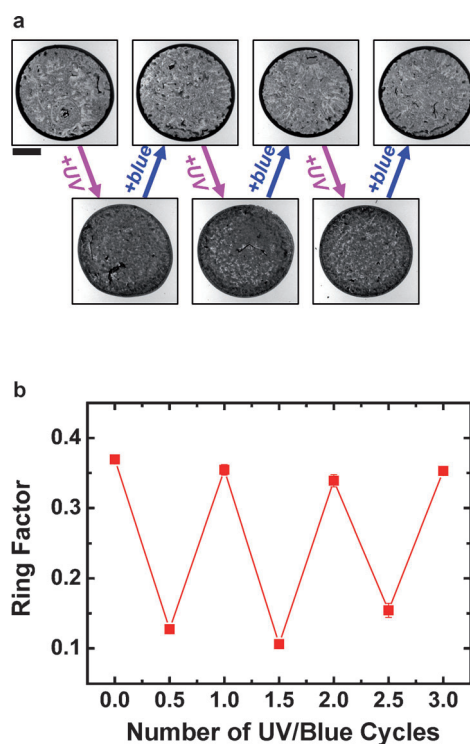


Figure 4. Successive UV/blue irradiation cycles induce reversible transitions between a disk- and a ring-shaped pattern. a) Representative micrographs of the deposits obtained for [AzoTAB]=1 mM and successive irradiations at 365 nm for 60 seconds (+UV) and at 440 nm for 60 seconds (+blue) on 1 μL drops. The full evaporation time was approximately 10 minutes. Scale bar: 500 μm . b) RF values, computed according to Figure S5, for successive UV/blue light irradiation cycles. Symbols and error bars show mean \pm SD values for three drops.

all kinds of interfaces or in bulk media^[14] in a non-invasive, highly flexible, and straightforward way.

Received: July 4, 2014

Revised: August 20, 2014

Published online: October 6, 2014

Keywords: coffee-ring effect · evaporation · photocontrol · photoisomerization · surfactants

- [1] a) R. D. Deegan, O. Bakajin, T. F. Dupont, G. Huber, S. R. Nagel, T. A. Witten, *Nature* **1997**, *389*, 827–829; b) W. Sempels, R. De Dier, H. Mizuno, J. Hofkens, J. Vermant, *Nat. Commun.* **2013**, *4*, 1757; c) Y. Deng, X.-Y. Zhu, T. Kienlen, A. Guo, *J. Am. Chem. Soc.* **2006**, *128*, 2768–2769; d) I. Smalyukh, O. Zribi, J. Butler, O. Lavrentovich, G. Wong, *Phys. Rev. Lett.* **2006**, *96*, 177801.
- [2] a) Z. Q. Lin, S. Granick, *J. Am. Chem. Soc.* **2005**, *127*, 2816–2817; b) R. Duggal, F. Hussain, M. Pasquali, *Adv. Mater.* **2006**, *18*, 29–34; c) Z. Zhang, X. Zhang, Z. Xin, M. Deng, Y. Wen, Y. Song, *Adv. Mater.* **2013**, *25*, 6714–6718; d) M. Layani, M. Gruchko, O. Milo, I. Balberg, D. Azulay, S. Magdassi, *ACS Nano* **2009**, *3*, 3537–3542; e) D. J. Harris, H. Hu, J. C. Conrad, J. A. Lewis, *Phys. Rev. Lett.* **2007**, *98*, 148301; f) J. Xu, J. Xia, S. W. Hong, Z. Lin, F. Qiu, Y. Yang, *Phys. Rev. Lett.* **2006**, *96*, 066104; g) S. W. Hong, J. Wang, Z. Lin, *Angew. Chem. Int. Ed.* **2009**, *48*,

- 8356–8360; *Angew. Chem.* **2009**, *121*, 8506–8510; h) W. Han, M. Byun, B. Li, X. Pang, Z. Lin, *Angew. Chem. Int. Ed.* **2012**, *51*, 12588–12592; *Angew. Chem.* **2012**, *124*, 12756–12760; i) W. Han, Z. Lin, *Angew. Chem. Int. Ed.* **2012**, *51*, 1534–1546; *Angew. Chem.* **2012**, *124*, 1566–1579; j) W. Han, M. He, M. Byun, B. Li, Z. Lin, *Angew. Chem. Int. Ed.* **2013**, *52*, 2564–2568; *Angew. Chem.* **2013**, *125*, 2624–2628; k) B. Li, W. Han, B. Jiang, Z. Lin, *ACS Nano* **2014**, *8*, 2936–2942.
- [3] Y. Kim, G. B. Hurst, M. J. Doktycz, M. V. Buchanan, *Anal. Chem.* **2001**, *73*, 2617–2624.
- [4] a) R. G. Larson, *Angew. Chem. Int. Ed.* **2012**, *51*, 2546–2548; *Angew. Chem.* **2012**, *124*, 2596–2598; b) H. B. Eral, D. M. Augustine, M. H. G. Duits, F. Mugele, *Soft Matter* **2011**, *7*, 4954–4958.
- [5] a) R. Bhardwaj, X. H. Fang, P. Somasundaran, D. Attinger, *Langmuir* **2010**, *26*, 7833–7842; b) H. Hu, R. G. Larson, *J. Phys. Chem. B* **2006**, *110*, 7090–7094; c) A. Crivoi, F. Duan, *Phys. Rev. E* **2013**, *87*, 042303.
- [6] a) T. Still, P. J. Yunker, A. G. Yodh, *Langmuir* **2012**, *28*, 4984–4988; b) M. Majumder et al., *J. Phys. Chem. B* **2012**, *116*, 6536–6542; c) V. Nguyen, K. Stebe, *Phys. Rev. Lett.* **2002**, *88*, 164501; d) D. M. Kuncicky, O. D. Velev, *Langmuir* **2008**, *24*, 1371–1380.
- [7] a) P. J. Yunker, T. Still, M. A. Lohr, A. G. Yodh, *Nature* **2011**, *476*, 308–311; b) C. Monteux, F. Lequeux, *Langmuir* **2011**, *27*, 2917–2922.
- [8] a) A. Diguët, R.-M. Guillemic, N. Magome, A. Saint-Jalmes, Y. Chen, K. Yoshikawa, D. Baigl, *Angew. Chem. Int. Ed.* **2009**, *48*, 9281–9284; *Angew. Chem.* **2009**, *121*, 9445–9448; b) A. Diguët, H. Li, N. Queyriaux, Y. Chen, D. Baigl, *Lab Chip* **2011**, *11*, 2666–2669; c) A. Venancio-Marques, F. Barbaud, D. Baigl, *J. Am. Chem. Soc.* **2013**, *135*, 3218–3223; d) A. Venancio-Marques, D. Baigl, *Langmuir* **2014**, *30*, 4207–4212.
- [9] P. Connor, R. Ottewill, *J. Colloid Interface Sci.* **1971**, *37*, 642–651.
- [10] S. Rudiuk, K. Yoshikawa, D. Baigl, *J. Colloid Interface Sci.* **2012**, *368*, 372–377.
- [11] a) P. Petit, I. Javierre, P.-H. Jézéquel, A.-L. Biance, *Cem. Concr. Res.* **2014**, *60*, 37–44; b) R. Deleurence, C. Parneix, C. Monteux, *Soft Matter* **2014**, *10*, 7088–7095.
- [12] A. Diguët, N. K. Mani, M. Geoffroy, M. Sollogoub, D. Baigl, *Chem. Eur. J.* **2010**, *16*, 11890–118906.
- [13] V. R. Dugyala, M. G. Basavaraj, *Langmuir* **2014**, *30*, 8680–8686.
- [14] a) Z. Niu, J. He, T. P. Russell, Q. Wang, *Angew. Chem. Int. Ed.* **2010**, *49*, 10052–10066; *Angew. Chem.* **2010**, *122*, 10250–10265; b) Y. Cui, M. T. Björk, J. A. Liddle, C. Sönnichsen, B. Boussert, A. P. Alivisatos, *Nano Lett.* **2004**, *4*, 1093–1098; c) G. M. Whitesides, B. Grzybowski, *Science* **2002**, *295*, 2418–2421; d) J. Palacci, S. Sacanna, A. P. Steinberg, D. J. Pine, P. M. Chaikin, *Science* **2013**, *339*, 936–940; e) T. P. Bigioni, X.-M. Lin, T. T. Nguyen, E. I. Corwin, T. A. Witten, H. M. Jaeger, *Nat. Mater.* **2006**, *5*, 265–270.